$\alpha + \alpha + t$ cluster structures and ^{12}C(0_2^+)-analog states in ^{11}B

Taiichi Yamada
Laboratory of Physics, Kanto Gakuin University, Yokohama 236-8501, Japan

Yasuro Funaki
Institute of Physics, University of Tsukuba, Tsukuba 305-8571, Japan

(Received 22 July 2010; revised manuscript received 2 November 2010; published 27 December 2010)

The structure of $3/2^-$ and $1/2^+$ states in ^{11}B is investigated with an $\alpha + \alpha + t$ orthogonality condition model (OCM) based on the Gaussian expansion method. Full levels up to the $3/2_3^-$ and $1/2_2^+$ states around the $\alpha + \alpha + t$ threshold ($E_x = 11.1$ MeV) are reproduced consistently with the experimental energy levels. It is shown that the $3/2_3^-$ state located around the ^{7}Li + α threshold has an $\alpha + \alpha + t$ cluster structure, whereas the $3/2_1^-$ and $3/2_2^-$ states have a shell-model-like compact structure. We found that the $3/2_3^-$ state does not possess an α-condensate-like nature analogous to the 0_2^+ state of ^{12}C (Hoyle state) which has a dilute 3α-condensate structure described by a $(0S_\alpha)^3$ configuration with about 70% probability, although the monopole transition strength of the former is as large as that of the latter. We discuss the reasons why the $3/2_3^-$ state does not have the condensate character. On the other hand, the $1/2_1^+$ state just below the ^{7}Li + α threshold has a cluster structure that can be interpreted as a parity-doublet partner of the $3/2_3^-$ state. We indicate that the 12.56-MeV state ($J^\pi = 1/2_2^+$) just above the $\alpha + \alpha + t$ threshold observed in the ^{7}Li(^{7}Li,^{11}B*)t reaction, etc., is of the dilute cluster-gas-like configuration and is a strong candidate for *the product states of clusters*, having a configuration of $(0S_\alpha)^2(0S_t)$ with about 65% probability, from the analyses of the single-cluster motions in ^{11}B. The structure property of the $1/2^+$ resonant state is analyzed with the complex scaling method.

DOI: 10.1103/PhysRevC.82.064315 PACS number(s): 21.10.Dr, 21.10.Gv, 21.60.Gx, 03.75.Hh

I. INTRODUCTION

The cluster picture as well as the mean-field picture is important to understand the structure of light nuclei [1,2]. The Hoyle state (the 0_2^+ state at $E_x = 7.65$ MeV in ^{12}C) is a typical cluster state with the 3α-cluster structure [3,4], which appears by only 0.38 MeV above the 3α threshold and is characterized by the large monopole transition rate sharing about 16% of the energy-weighted sum rule [5]. The Hoyle state has been reinvestigated from the viewpoint of the α condensation [6]. The definitions and occurrences of the nuclear α-particle condensation are discussed in detail in Ref. [7]. Many theoretical works have shown that the Hoyle state has a 3α-condensate-like structure [6–13], in which the 3α particles occupy an identical $0S$ orbit with 70% probability [9,10], forming a dilute α-gas-like configuration with $(0S_\alpha)^3$, that is, the product states of three α's.

The structure study of ^{16}O has recently made a great advance. The six lowest 0^+ states of ^{16}O have very nicely been reproduced up to about 15 MeV excitation energy, including the ground state, with the 4α orthogonality condition model (OCM) [14]. The OCM is a semimicroscopic cluster model, which is an approximation of the resonating group method (RGM) and is extensively described in Ref. [15]. Many successful applications of the OCM are reported in Ref. [2]. The 4α OCM calculation showed that the 0_6^+ state around the 4α threshold is a strong candidate of the 4α-particle condensate state, having a large α-condensate fraction of 60% for the α-gas-like configuration $(0S_\alpha)^4$ as well as a large component of the $\alpha + ^{12}$C(0_2^+) configuration. The 0_6^+ state could be called the product states of four α particles. In this article the terminology of "product states of α particles" is used, instead of "Hoyle-analog states," because the 0_2^+ state in ^{12}C is called the "Hoyle state" for historical reasons, not for physical reasons [16,17]. The α-cluster product states heavier than ^{16}O are predicted to exist around their α-cluster-disintegrated thresholds in self-conjugate $A = 4n$ nuclei [6,18,19].

Besides the $4n$ nuclei, one can also expect cluster-gas states composed of α and triton clusters (including valence neutrons, etc.) around their cluster-disintegrated thresholds in $A \neq 4n$ nuclei, in which all clusters are in their respective $0S$ orbits, similar to the Hoyle state with $(0S_\alpha)^3$. The states, thus, can be called *product states of clusters* in the non-self-conjugated nuclei. It is an intriguing subject to investigate whether or not the product states of clusters exist in $A \neq 4n$ nuclei, for example, ^{11}B, composed of 2α and t clusters.

The cluster structure in ^{11}B was studied about 30 years ago with the $\alpha + \alpha + t$ OCM using the harmonic oscillator basis by Nishioka *et al.* [20–22]. They found that (1) the $3/2_3^-$ state ($E_x = 8.6$ MeV) just below the ^{7}Li + α threshold has a well-developed molecular-like structure of ^{7}Li(g.s) + α, where ^{7}Li(g.s) denotes the ground state of ^{7}Li with the $\alpha + t$ cluster structure, and (2) the $3/2_1^-$ (g.s) and $3/2_2^-$ ($E_x =$ 5.0 MeV) states have shell-model-like compact structures. The model space adopted in Refs. [20–22], however, was not sufficient to account simultaneously for the ^{7}Li + α cluster configuration as well as the $\alpha + \alpha + t$ gas-like configuration. In addition, limited experimental data in those days caused difficulties in giving the definite conclusion that the $3/2_3^-$ state has an $\alpha + \alpha + t$ cluster structure.

Kawabata and his collaborators have investigated the excited states of ^{11}B by using the ^{11}B(d,d') reaction [23]. They eventually concluded that the $3/2_3^-$ state at $E_x = 8.56$ MeV

has an α-cluster structure. Among many reasons for this conclusion, one is a large isoscalar monopole transition rate for the $3/2^-_3$ state, $B(E0{:}\mathrm{IS}) = 96 \pm 16$ fm^4, which is of a value similar to that for the Hoyle state in ^{12}C, $B(E0{:}\mathrm{IS}) = 120 \pm 9$ fm^4. A close relation between large isoscalar monopole strengths and underlying cluster structures in excited states was discussed by the present authors and their co-workers (see Ref. [5]). According to the literature, the largeness of the isoscalar monopole transition rate for $3/2^-_3$ originates from the fact that the state has a cluster structure.

Another reason why the $3/2^-_3$ state has the cluster structure is that the AMD (antisymmetrized molecular dynamics) calculation [23,24] has reproduced the large monopole transition rate for the $3/2^-_3$ state and has succeeded in assigning an $\alpha + \alpha + t$ cluster structure to this state. Comparing the density distribution of the $3/2^-_3$ state (calculated by AMD) with that of the Hoyle state (together with the analysis of the expectation values of the harmonic oscillator quanta in their wave functions), the AMD calculation [24] claimed that the $3/2^-_3$ state has a clustering feature similar to that of the Hoyle state. However, the single-cluster properties such as single-cluster orbits and their occupation probabilities in the $3/2^-_3$ state were not studied. Their quantities are independent of the information of the density distribution and the expectation values of the harmonic oscillator quanta in the wave function. Thus, it is very important to study the single-cluster properties in order to judge whether the $3/2^-_3$ state possesses the similarity to the Hoyle state with the $(0S_\alpha)^3$-like structure. As discussed in Refs. [9,10,25,26], the single-cluster motions such as α (t)-cluster orbits and their occupation probabilities in a nuclear state can be investigated by solving the eigenvalue equation of the single-cluster density matrix $\rho(\boldsymbol{r}, \boldsymbol{r}')$ derived from the microscopic and/or semimicroscopic wave functions.

The purpose of the present article is to study the structure of $3/2^-$ and $1/2^+$ states in ^{11}B up to around the $\alpha + \alpha + t$ threshold. Here we take the $\alpha + \alpha + t$ OCM with the Gaussian expansion method (GEM), the model space of which is large enough to cover the $\alpha + \alpha + t$ gas, the $^7\mathrm{Li} + \alpha$ cluster, and the shell-model configurations. Combining the OCM and the GEM provides a powerful method to study the structure of light nuclei [9,12,27] as well as light hypernuclei [28,29], because the Pauli-blocking effect among the clusters is properly taken into account by the OCM and the GEM covers an approximately complete model space [30,31]. This framework can treat precisely a strong parity dependence of the α-t potential. The negative-parity potential is attractive enough to make bound states ($3/2^-_1$ and $1/2^-_1$) and resonant states ($7/2^-_1$ and $5/2^-_1$) of ^{7}Li, whereas the positive-parity potential is not. This parity dependence should play an important role in producing the cluster states of ^{11}B, as will be discussed later. The single-cluster properties such as single-α-particle (single-t-particle) orbits and occupation probabilities are investigated to judge whether or not the $3/2^-_3$ state is described by the product states of clusters, similar to the Hoyle state with $(0S)^3_\alpha$, by solving the eigenvalue equation of the single-cluster density matrix $\rho(\boldsymbol{r}, \boldsymbol{r}')$ derived from the total wave function of ^{11}B. The resonance structure of $1/2^+$ states is also studied with the complex scaling method (CSM), since they appear around the $\alpha + \alpha + t$ threshold with $E_x = 11.1$ MeV.

It is also interesting to explore the product states of clusters with the $\alpha + \alpha + t$ structure in $1/2^+$ states, because one can conjecture an appearance of the product state, $(0S_\alpha)^2(0S_t)$, in $J^\pi = 1/2^+$ of ^{11}B ($1/2$ comes from the spin of the triton) from the similarity of $(0S_\alpha)^3$ in the Hoyle state. The structure of the positive-parity states (isospin $T = 1/2$) in ^{11}B so far has not been discussed well in AMD [24] and the noncore shell model [32]. Recently several positive-parity states of ^{11}B with $T = 1/2$ have been observed with the ^{7}Li(^{9}Be,α^7Li)^{5}He reaction [33], the ^{7}Li(^{7}Li,^{11}B*)t reaction [34], and the decay-particle measurements of $\alpha + {}^7$Li and $t + {}^8$Be from excited ^{11}B* states [35]. An interesting result in these experiments is as follows: The $1/2^+(3/2^+)$ state at $E_x = 12.56$ MeV, which has been identified so far as the isospin $T = 3/2$ state [36], is observed through the $\alpha + {}^7$Li decay channel [33–35]. It was concluded that the 12.56-MeV state has isospin $T = 1/2$ or alternatively it is observed at an energy similar to that of $T = 3/2$. Therefore, it is interesting to investigate theoretically the structure of the 12.56-MeV state.

The present article is organized as follows. In Sec. II we formulate the $\alpha + \alpha + t$ OCM with the GEM as well as the CSM. Section III is devoted to results and discussion. Finally we present the summary in Sec. IV.

II. FORMULATION

In this section, we present the formulation of the $\alpha + \alpha + t$ OCM with the GEM for ^{11}B, and give a brief formulation of the CSM with the $\alpha + \alpha + t$ OCM to study the resonant structures of ^{11}B.

A. $\alpha + \alpha + t$ OCM with the Gaussian expansion method

The total wave function of ^{11}B (the total angular momentum J and total isospin $T = 1/2$) within the frame of the $\alpha + \alpha + t$ OCM is expanded in terms of the Gaussian basis,

$$\begin{aligned}\Phi_J(^{11}\mathrm{B}) = &\sum_c \sum_{\nu,\mu} A_c(\nu,\mu)\Phi_c^{(12,3)}(\nu,\mu) \\ &+ \sum_c \sum_{\nu,\mu} B_c(\nu,\mu)\left[\Phi_c^{(23,1)}(\nu,\mu)\right. \\ &\left. + \Phi_c^{(31,2)}(\nu,\mu)\right], \qquad (1)\end{aligned}$$

$$\Phi_c^{(ij,k)}(\nu,\mu) = \left\{\left[\varphi_\ell(\boldsymbol{r}_{ij},\nu)\varphi_\lambda(\boldsymbol{r}_k,\mu)\right]_L \chi_{\frac{1}{2}}(t)\right\}_J, \qquad (2)$$

$$\varphi_\ell(\boldsymbol{r},\nu) = N_\ell(\nu) r^\ell \exp(-\nu r^2) Y_\ell(\hat{\boldsymbol{r}}), \qquad (3)$$

where we assign the cluster numbers as 1 and 2 for the two α clusters (spin 0) and 3 for the t cluster (spin 1/2). $\Phi_J^{(12,3)}$ [$\Phi_J^{(23,1)+(31,2)}$] denotes the relative wave function of the $\alpha + \alpha + t$ system with the Jacobi-coordinate system shown in Fig. 1(a) [Figs. 1(b) and 1(c)]. It is noted that $\Phi_J^{(23,1)+(31,2)}$ is symmetric with respect to the particle-number exchange between 1 and 2. N_ℓ is the normalization factor of the Gaussian basis φ_ℓ, and $\boldsymbol{r}_{ij}$ ($\boldsymbol{r}_k$) denotes the relative coordinate between the ith and jth clusters (the kth cluster and the center-of-mass coordinate of the ith and jth clusters). The angular momentum channel is presented as $c = [(\ell,\lambda)_L \frac{1}{2}]_J$, where ℓ (λ) denotes

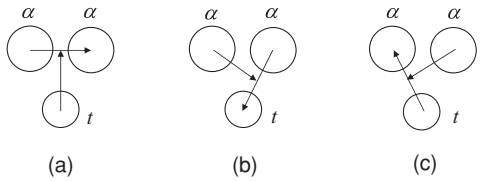

FIG. 1. Three-Jacobi-coordinate systems in the $\alpha+\alpha+t$ model.

the relative orbital angular momentum with respect to $\boldsymbol{r}_{ij}$ ($\boldsymbol{r}_k$), and L ($\frac{1}{2}$) is the total orbital angular momentum (the spin of t particles). The Gaussian parameter ν is taken to be of geometrical progression,

$$\nu_n = 1/b_n^2, \quad b_n = b_{\min}a^{n-1}, \quad n = 1 \sim n_{\max}. \tag{4}$$

It is noted that this prescription is found to be very useful in optimizing the ranges with a small number of free parameters with high accuracy [30,37].

The total Hamiltonian for the $\alpha+\alpha+t$ system is presented as

$$\mathcal{H} = \sum_{i=1}^{3} T_i - T_{\text{c.m.}} + V_{2\alpha}^{(\text{N})}(r_{12}) + V_{2\alpha}^{(\text{C})}(r_{12}) + \sum_{i=1}^{2}\left[V_{\alpha t}^{(\text{N})}(r_{i3}) + V_{\alpha t}^{(\text{C})}(r_{i3})\right] + V_{2\alpha t} + V_{\text{Pauli}}, \tag{5}$$

where T_i, $V_{2\alpha}^{(\text{N})}$ ($V_{\alpha t}^{(\text{N})}$), and $V_{2\alpha t}$ stand for the kinetic energy operator for the ith cluster, α-α (α-t) potential, and three-body potential, respectively, and $V_{2\alpha}^{(\text{C})}$ ($V_{\alpha t}^{(\text{C})}$) is the Coulomb potential between 2α clusters (α and t). The center-of-mass kinetic energy ($T_{\text{c.m.}}$) is subtracted from the Hamiltonian. The Pauli-blocking operator V_{Pauli} [38] is expressed as

$$V_{\text{Pauli}} = \lim_{\lambda\to\infty} \lambda \hat{O}_{\text{Pauli}}, \tag{6}$$

$$\hat{O}_{\text{Pauli}} = \sum_{2n+\ell<4,\ell=\text{even}} |u_{n\ell}(\boldsymbol{r}_{12})\rangle\langle u_{n\ell}(\boldsymbol{r}_{12})| + \sum_{2n+\ell<3}\sum_{i=1}^{2} |u_{n\ell}(\boldsymbol{r}_{i3})\rangle\langle u_{n\ell}(\boldsymbol{r}_{i3})| \tag{7}$$

which removes the Pauli forbidden states between the two α particles in $0S$, $0D$, and $1S$ states as well as those between α and t particles in $0S$, $0P$, $0D$, and $1S$ states. Consequently, the ground state with the shell-model-like configuration can be described properly in the present model.

Here we remind the reader that Refs. [20,21] don't contain the Pauli-blocking operator V_{Pauli} (6). The reason for this is given as follows. In Refs. [20,21], the total wave function of ^{11}B, $\Phi_J(^{11}\text{B})$, is expanded in terms of the Pauli-allowed states constructed by the harmonic oscillator wave functions. The Pauli-allowed states can be classified with the total harmonic oscillator quanta Q and the SU(3) representation (λ, μ) (see Table I in Ref. [20]). Thus, they don't need to use the Pauli-blocking operator in their calculation. However, the number of the Pauli-allowed states increases very rapidly with increasing the value of Q. This is the reason why they adapted only the small model space. This is a major fault of using the harmonic oscillator basis, because one needs a significantly large model space specified by Q in order to describe the $\alpha+\alpha+t$ gas-like structure. In fact, in the case of the Hoyle state, we found over 100 quanta to describe the 3α-gas-like structure, but the quanta were not enough to reach a numerical convergence [5,27]. On the other hand, the Gaussian basis in Eqs. (1)–(3) is found to have major merit in that an optimum smaller model space can describe the gas-like structure as well as the compact shell-model-like structure with a good numerical convergence. In the Gaussian basis, we have to remove the Pauli-forbidden states from the total wave function $\Phi_J(^{11}\text{B})$ by introducing the method of Kukulin *et al.* [38], that is, introducing the Pauli-blocking operator (6) into the Hamiltonian as mentioned above.

The effective α-α potential and Coulomb potential, $V_{2\alpha}^{(\text{N})}$ and $V_{2\alpha}^{(\text{C})}$, in Eq. (5) are constructed with the folding procedure, where we fold the modified Hasegawa-Nagata effective NN interaction (MHN) [39] and the pp Coulomb potential with the α-particle density. They reproduce the observed $\alpha\alpha$ scattering phase shifts (S, D, and G waves) and the energies of the ^{8}Be ground state and of the Hoyle state (0_2^+ in ^{12}C) [9,12]. Concerning the effective α-t potential and Coulomb potentials, we use the folding potentials, which reproduce well the low-lying energy spectra of ^{7}Li [$3/2_1^-$ (g.s.), $1/2_1^-$, $7/2_1^-$, and $5/2_1^-$] (including the low-energy α-t scattering phase shifts) obtained initially by Nishioka *et al.* [20,21]. The potentials are applied to the structure study of $^7_\Lambda$Li with the $\alpha+t+\Lambda$ model and are known to reproduce well the low-lying structure of the hypernucleus [28,29]. We made a fine tuning for the α-t potential obtained by Nishioka *et al.* [20,21] so as to get a qualitatively better agreement with the experimental phase shifts. Note that the α-t potential has a strong parity-dependence: The odd-parity potentials are attractive to reproduce the bound states ($3/2^-$, $1/2^-$) with respect to the $\alpha+t$ threshold, while the even-parity potentials are weakly attractive and thus no bound and/or resonant states with positive parity have been observed in low-energy excitation region up to $E_x \sim 15$ MeV [40].

The three-body potential $V_{2\alpha t}$ is introduced phenomenologically so as to reproduce the energies of the ground state ($3/2_1^-$) and the first excited positive-parity state ($1/2_1^+$) of ^{11}B with respect to the $\alpha+\alpha+t$ threshold. The origin of $V_{2\alpha t}$ is considered to derive from the state dependence of the effective nucleon-nucleon interaction and an additional Pauli repulsion arising from exchanging nucleons among the three clusters ($\alpha+\alpha+t$). It should be short range and hence only act in compact configurations. In the present article, we take the following phenomenological three-body potential,

$$V_{2\alpha t} = \sum_{Q=7,8} V_0(Q) \sum_{(\lambda\mu)} \sum_{L^\pi} \left|\Phi^{\text{SU(3)}}_{(\lambda\mu)Q}(L^\pi)\right\rangle\left\langle\Phi^{\text{SU(3)}}_{(\lambda\mu)Q}(L^\pi)\right|, \tag{8}$$

where $\Phi^{\text{SU(3)}}_{(\lambda\mu)Q}(L^\pi)$ with the total orbital angular momentum L represents the SU(3)[443]$(\lambda\mu)$ wave function with the total oscillator quanta Q ($Q \geqslant 7$). It is noted that the present $\alpha+\alpha+t$ model space can be classified into the SU(3) bases with the irreducible representation, $(\lambda\mu)Q$, with partition $[f] = [443]$, and the total wave function of ^{11}B with positive

(negative) parity in Eq. (1) can be expanded in terms of the $\Phi^{SU(3)}_{(\lambda\mu)Q}(L^\pi)$ bases with even (odd) Q values [20,21]. The $(\lambda\mu) = (13)$ basis with $Q = 7$ is a unique Pauli allowed state for negative-parity states of ^{11}B with $Q = 7$, which is equivalent to the shell-model configuration of $(0s)^4(0p)^7$. Thus this SU(3) basis becomes the main component in the ground state of ^{11}B. On the other hand, there exist only three Pauli-allowed states, $(\lambda\mu) = (42)$, (23), and (04), for the positive-parity states with $Q = 8$. Therefore they correspond to the main components in the first excited states with even parity in the present model. For simplicity, the strengths of the three-body potential, $V_0(Q = 7)$ and $V_0(Q = 8)$, are fixed so as to reproduce the experimental energies of the ground state of ^{11}B and the first $1/2^+$ state ($E_x = 6.79$ MeV), respectively, with respect to the $\alpha + \alpha + t$ threshold: $V_0(Q = 7) = 10.2$ MeV and $V_0(Q = 8) = 4.5$ MeV. The expectation value of this three-body potential does not exceed 8% of that of the corresponding two-body term, even for the ground state with the most compact structure, that is, being the most sensitive to the potential. When we switch off the three-body potential, the shell-model-like states such as $3/2^-_1$ and $3/2^-_2$ states are overbound by 9.5 MeV, while the $1/2^+_1$ state is overbound by 2.9 MeV, and the energy levels of $3/2^-_3$ and $1/2^+_2$ stay pretty much the same (see Fig. 2). This overbinding in $3/2^-_1$ and $3/2^-_2$ was also observed in the previous study [20,21].

The equation of motion of ^{11}B with the $\alpha + \alpha + t$ OCM is obtained by the variational principle,

$$\delta[\langle\Phi_J(^{11}\mathrm{B}) \mid \mathcal{H} - E \mid \Phi_J(^{11}\mathrm{B})\rangle] = 0, \tag{9}$$

where E denotes the eigenenergy of ^{11}B measured from the $\alpha + \alpha + t$ threshold. The energy E and expansion coefficients A_c and B_c in the total wave function shown in Eq. (1) are determined by solving a secular equation derived from Eq. (9).

It is instructive to study single-α-particle (single-t-particle) orbits and corresponding occupation probabilities in ^{11}B. We

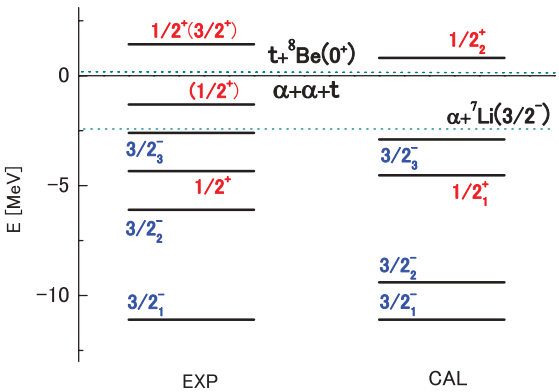

FIG. 2. (Color online) Calculated energy levels of $3/2^-$ and $1/2^+$ states in ^{11}B with respect to the $\alpha + \alpha + t$ threshold together with the experimental data [36]. The thresholds of the $\alpha + {}^7\mathrm{Li}(3/2^-)$ and $t + {}^8\mathrm{Be}(0^+)$ channels are shown in the figure. It is noted that the threshold energies of the $\alpha + {}^7\mathrm{Li}(1/2^-)$, $\alpha + {}^7\mathrm{Li}(7/2^-)$, $\alpha + {}^7\mathrm{Li}(5/2^-)$, and $t + {}^8\mathrm{Be}(2^+)$ channels are $E = -1.99$, 2.19, 4.14, and 3.12 MeV, respectively.

define the single-cluster density matrices for α and t clusters, respectively, as

$$\rho^{(\alpha)}(\boldsymbol{r}, \boldsymbol{r}') = \langle\Phi_J(^{11}\mathrm{B})|\frac{1}{2}\sum_{i=1}^{2}\left|\delta\left(\boldsymbol{r}_i^{(G)} - \boldsymbol{r}'\right)\right\rangle \times \left\langle\delta\left(\boldsymbol{r}_i^{(G)} - \boldsymbol{r}\right)\right|\Phi_J(^{11}\mathrm{B})\rangle, \tag{10}$$

$$\rho^{(t)}(\boldsymbol{r}, \boldsymbol{r}') = \langle\Phi_J(^{11}\mathrm{B})|\left|\delta\left(\boldsymbol{r}_3^{(G)} - \boldsymbol{r}'\right)\right\rangle \times \left\langle\delta\left(\boldsymbol{r}_3^{(G)} - \boldsymbol{r}\right)\right|\Phi_J(^{11}\mathrm{B})\rangle, \tag{11}$$

where $\boldsymbol{r}_i^{(G)}$ $(i = 1, 2)$ $[\boldsymbol{r}_3^{(G)}]$ represents the coordinate vector of the ith α (triton) cluster with respect to the center-of-mass coordinate of the $\alpha + \alpha + t$ system. The calculated method of ρ is given in Refs. [9,10,25,26]. The single-α-particle (single-t-particle) orbits and corresponding occupation probabilities are obtained by solving the eigenvalue equation of the single-cluster density matrices,

$$\int d\boldsymbol{r}\,\rho^{(\alpha)}(\boldsymbol{r}, \boldsymbol{r}')f_\mu^{(\alpha)}(\boldsymbol{r}') = \mu^{(\alpha)}f_\mu^{(\alpha)}(\boldsymbol{r}), \tag{12}$$

$$\int d\boldsymbol{r}\,\rho^{(t)}(\boldsymbol{r}, \boldsymbol{r}')f_\mu^{(t)}(\boldsymbol{r}') = \mu^{(t)}f_\mu^{(t)}(\boldsymbol{r}), \tag{13}$$

where the eigenvalue $\mu^{(\alpha)}$ $(\mu^{(t)})$ denotes the occupation probability for the corresponding single-cluster orbit $f_\mu^{(\alpha)}$ $(f_\mu^{(t)})$ with the argument of the intrinsic coordinate of an arbitrary α (triton) cluster in a nucleus measured from the center-of-mass coordinate of ^{11}B. The spectrum of the occupation probabilities provides important information on the occupancies of the single-α-(t-)particle orbit in ^{11}B. If the two α particles (one t particle) occupy only a single orbit, the occupation probability for this orbit becomes 100%.

The nuclear root-mean-square (rms) radius of ^{11}B in the present OCM is given as

$$R_N = \left[\tfrac{1}{11}\left(2\langle r^2\rangle_\alpha + \langle r^2\rangle_t + 2{R_{\alpha-\alpha}}^2 + \tfrac{24}{11}{R_{^8\mathrm{Be}-t}}^2\right)\right]^{1/2}, \tag{14}$$

where $R_{\alpha-\alpha}$ $(R_{^8\mathrm{Be}-t})$ presents the rms distance between α and α (^{8}Be and t) in ^{11}B. In Eq. (14) we take into account the finite size effect of α and t clusters, where the experimental rms radii for the α and t particles are used in $\sqrt{\langle r^2\rangle_\alpha}$ and $\sqrt{\langle r^2\rangle_t}$, respectively.

The reduced width amplitude or overlap amplitude is useful to see the degree of clustering in the nucleus. In the present article, we study the reduced width amplitudes for the $^7\mathrm{Li} + \alpha$ and $^8\mathrm{Be} + t$ channels, respectively, defined as

$$\mathcal{Y}^{^7\mathrm{Li}-\alpha}_{J_7\ell_{74}J}(r_{74}) = r_{74} \times \left\langle\left[\frac{\delta(r'_{74} - r_{74})}{{r'_{74}}^2}\phi_{J_7}(^7\mathrm{Li})Y_{\ell_{74}}(\hat{\boldsymbol{r}}'_{74})\right]_J \times \left|\Phi_J(^{11}\mathrm{B})\right\rangle, \tag{15}$$

$$\mathcal{Y}^{^8\mathrm{Be}-t}_{J_8(\ell_{83}\frac{1}{2})j_{83}J}(r_{83}) = r_{83} \times \left\langle\left[\frac{\delta(r'_{83} - r_{83})}{{r'_{83}}^2}\phi_{J_8}(^8\mathrm{Be})[Y_{\ell_{83}}(\hat{\boldsymbol{r}}'_{83}) \times \chi_{\frac{1}{2}}(t)]_{j_{83}}\right]_J\left|\Phi_J(^{11}\mathrm{B})\right\rangle, \tag{16}$$

where r_{74} (r_{83}) denotes the radial part of the relative coordinate between ^{7}Li and α (^{8}Be and t). The wave function $\phi_{J_7}(^7\mathrm{Li})$ [$\phi_{J_8}(^8\mathrm{Be})$] of ^{7}Li (^{8}Be) with the total angular momentum J_7 (J_8) is obtained with the $\alpha+t$ OCM ($\alpha+\alpha$ OCM). The spectroscopic factor S^2 is defined as

$$S^2=\int_0^\infty dr[\mathcal{Y}(r)]^2, \tag{17}$$

where $\mathcal{Y}$ denotes the reduced width amplitude.

B. Complex-scaling method with $\alpha+\alpha+t$ OCM

The CSM is taken to study the resonant structures of ^{11}B. The CSM is a powerful tool to investigate the resonant parameters (energies and widths) of the resonant states as well as the binding energies of the bound states [41]. Application of the CSM is easy in the framework of the $\alpha+\alpha+t$ OCM.

In the CSM, we transform the relative coordinates of the $\alpha+\alpha+t$ model shown in Fig. 1, $\{\boldsymbol{r}_{ij},\boldsymbol{r}_k\}$ with $(ij,k)=$ (12, 3), (23,1), and (32,1), by the operator U^θ as

$$U^\theta\boldsymbol{r}_{ij}=\boldsymbol{r}_{ij}e^{i\theta}\text{and}\quad U^\theta\boldsymbol{r}_k=\boldsymbol{r}_ke^{i\theta}, \tag{18}$$

where θ is a scaling angle. Then, the Hamiltonian in Eq. (5) is transformed into the complex-scaled Hamiltonian,

$$\mathcal{H}^\theta=U^\theta\mathcal{H}(U^\theta)^{-1}. \tag{19}$$

The corresponding complex-scaled Schrödinger equation is expressed as

$$\mathcal{H}^\theta\Phi^\theta_J=E\Phi^\theta_J, \tag{20}$$

$$\Phi^\theta_J=e^{(3/2)i\theta\times2}\Phi_J(\{\boldsymbol{r}_{ij}e^{i\theta},\boldsymbol{r}_ke^{i\theta}\}), \tag{21}$$

where Φ_J is given in Eq. (1). The eigenstates Φ^θ_J are obtained by solving the eigenvalue problem of $\mathcal{H}^\theta$ in Eq. (20). In the CSM, all the energy eigenvalues E of bound and unbound states are obtained on a complex energy plane, according to the so-called ABC theorem given by Aguilar, Combes, and Balslev [41]. In this theorem, it is proven that the boundary condition of Gamow resonances is transformed to the damping behavior at the asymptotic region. Thanks to this condition, the same theoretical method as that used for the bound states can be employed to obtain the many-body resonances. For ^{11}B, the continuum states of $^7\mathrm{Li}+\alpha$, $^8\mathrm{Be}+t$, and $\alpha+\alpha+t$ channels are obtained on the branch cuts rotated with the 2θ dependence [41]. On the contrary, bound states and resonances are discrete and obtainable independently of θ. Thus, these discrete states are located separately from the many-body continuum spectra on the complex energy plane. One can identify the resonance poles of complex eigenvalues: $E=E_r-i\Gamma/2$, where E_r and Γ are the resonance energy measured from the $\alpha+\alpha+t$ threshold and the decay width, respectively.

In the present study, we adapt the folding potentials for the α-α and α-t interactions in $\mathcal{H}$ in Eq. (19) (see also Sec. II A). The functional form of the folding potentials is analytically described in terms of the single Gaussian or the sum of the Gaussian functions, including the error function corresponding to the folding-type Coulomb potential. Thus, the CSM is applicable for the present model because our folding potentials are analytical [41].

In order to solve the complex-scaled Schrödinger equation, Eq. (20), we expand the wave function Eq. (21) in terms of the Gaussian basis functions shown in Eq. (1),

$$\Phi^\theta_J=\sum_c\sum_{\nu,\mu}F^\theta_c(\nu,\mu)\Phi^{(12,3)}_c(\nu,\mu)+\sum_c\sum_{\nu,\mu}G^\theta_c(\nu,\mu)\left[\Phi^{(23,1)}_c(\nu,\mu)\Phi^{(31,2)}_c(\nu,\mu)\right]. \tag{22}$$

The expansion coefficients $F^\theta_c(\nu,\mu)$ and $G^\theta_c(\nu,\mu)$ together with the discrete energy spectrum E are obtained by solving an eigenvalue problem derived from Eqs. (20) and (22) [42–44]. This complex scaling method with the Gaussian basis functions is known to give the high precision needed to maintain the numerical stability of the complex eigenvalue problem.

III. RESULTS AND DISCUSSION

The energy levels of $3/2^-$ and $1/2^+$ states in ^{11}B with respect to the $\alpha+\alpha+t$ threshold are shown in Fig. 2, which are obtained with the $\alpha+\alpha+t$ OCM using the GEM. In the present calculation, we found that three $3/2^-$ states and two $1/2^+$ states come out as either bound states against particle decays or resonant states.

A. $3/2^-$ states

First we discuss the structures of the three $3/2^-$ states. The $3/2^-_1$ state at $E=-11.1$ MeV measured from the $\alpha+\alpha+t$ threshold corresponds to the ground state of ^{11}B. The calculated nuclear radius is $R_N=2.22$ fm (see Table I), the value of which is in correspondence with the experimental data 2.43 ± 0.11 fm [36]. According to the analysis of the wave function, the main component of this state is $\mathrm{SU(3)}[f](\lambda,\mu)_L=[443](1,3)_1$ with $Q=7$ harmonic oscillator quanta (95%) and its dominant angular momentum channel is $(L,S)_J=(1,\frac{1}{2})_{\frac{3}{2}}$. Thus, this state has a compact shell-model-like structure, in which the two α and one t clusters are heavily overlapping and melting each other away (due to antisymmetrization among nucleons) to have a shell-model configuration. On the other hand, we found that the $3/2^-_2$ state at $E=-9.4$ MeV has also a compact shell-model-like structure with the dominant component of $\mathrm{SU(3)}(\lambda,\mu)_L=(1,3)_2$ with $Q=7$ and $(L,S)_J=(2,\frac{1}{2})_{\frac{3}{2}}$. The nuclear radius of this state is $R_N=2.23$ fm, the value of which is similar to that of the ground state. The energy difference between the $3/2^-_1$ and $3/2^-_2$ states is about 2 MeV, which is smaller than the experimental data (∼5 MeV). This feature is recovered if we take into account the SU(3)[4421] shell-model configuration in the present OCM model space (or adopting an extended $\alpha+\alpha+d+n$ model space in the cluster-model terminology), as pointed out by Nishioka *et al.* [20,21].

In addition to the two $3/2^-$ states discussed above, the $3/2^-_3$ state appears at $E_x=8.2$ MeV ($E=-2.9$ MeV with respect to the $\alpha+\alpha+t$ threshold). The nuclear radius of $3/2^-_3$ is $R_N=3.00$ fm. This value is about 30% larger than that of the ground state of ^{11}B and is consistent with the AMD calculation ($R_N=3.0$ fm) [24]. The rms distance between α and α [between ^{8}Be(2α) and t] is $R_{\alpha-\alpha}=4.47$ fm ($R_{^8\mathrm{Be}-t}=3.49$ fm). Note that the value of $R_{\alpha-\alpha}\sim4$ fm in the

TABLE I. Calculated nuclear radii (R_N), α–α rms distances ($R_{\alpha-\alpha}$), and ^{8}Be–t distances ($R_{^8\mathrm{Be}-t}$) for the $3/2^-$ states of ^{11}B together with their α–t and ^{7}Li–α rms distances ($R_{\alpha-t}$ and $R_{^7\mathrm{Li}-\alpha}$, respectively). They are given in units of fm.

J^π	R_N	$R_{\alpha-\alpha}$	$R_{^8\mathrm{Be}-t}$	$R_{\alpha-t}$	$R_{^7\mathrm{Li}-\alpha}$
$3/2_1^-$	2.22	2.45	2.14	2.47	2.13
$3/2_2^-$	2.23	2.49	2.17	2.51	2.17
$3/2_3^-$	3.00	4.47	3.49	4.15	3.82

ground state of ^{8}Be with the $\alpha+\alpha$ OCM calculation. Thus, the intracluster distance between the two α's in $3/2_3^-$ is a little bit larger than that in the ground state of ^{8}Be. In addition, the intracluster distance between the α and t clusters in $3/2_3^-$ is 4.15 fm (see Table I), which is also larger than that (3.5 fm) in the ground state of ^{7}Li($\alpha+t$).

To study the structure of $3/2_3^-$, it is interesting to compare the reduced width amplitudes or overlap amplitudes of the ^{7}Li(g.s) $+\alpha$ channel [^{8}Be(g.s) $+t$] defined in Eq. (15) [(16)] for the $3/2_3^-$ and $3/2_1^-$ states. The results are shown in Fig. 3. One sees that (1) the reduced width amplitudes of the ^{7}Li $+\alpha$ and ^{8}Be $+t$ channels in $3/2_3^-$ are enhanced and significantly larger than those in the ground state, in particular, in the outermost-peak region, and (2) the number of the nodes of their amplitudes in the former state increase by one larger than those in the latter. It is noted that the radial behaviors of the reduced width amplitudes in the ground state of ^{11}B are determined by the dominant nature of SU(3)$(\lambda,\mu)=(1,3)$ in its state. As for the S^2 factors in $3/2_3^-$, the ^{7}Li(g.s) $+\alpha$ channel with the relative orbital angular momentum $\ell_{74}=0$ has the largest value of 0.278 among all of the ^{7}Li $+\alpha$ channels, and the second (third) largest channel is the ^{7}Li(g.s) $+\alpha$ [^{7}Li($1/2^-$) $+\alpha$] channel ($\ell_{74}=2$) with $S^2=0.126$ (0.125), while the ^{8}Be(g.s) $+t$ channel with the relative angular momentum $j_{83}=3/2$ has the largest value of 0.102. In the $3/2_1^-$ state, the corresponding S^2 factors are 0.144, 0.062, 0.052, and 0.062, respectively, for ^{7}Li(g.s) $+\alpha$ ($\ell_{74}=0$), ^{7}Li(g.s) $+\alpha$ ($\ell_{74}=2$), ^{7}Li($1/2^-$) $+\alpha$ ($\ell_{74}=2$), and ^{8}Be(g.s) $+t$ ($j_{83}=3/2$). Consequently, the $3/2_3^-$ state has an $\alpha+\alpha+t$ cluster structure, although the cluster structure of the $\alpha+t$ part is significantly distorted from that of the ground state of ^{7}Li.

Kawabata *et al.* measured the isoscalar monopole transition rate $B(E0{:}\mathrm{IS})$ for $3/2_3^-$ with the ^{11}B(d,d') reaction [23]. The experimental value is as large as 96 ± 16 fm^4, comparable to that of the Hoyle state in ^{12}C [$B(E0{:}\mathrm{IS})=120\pm9$ fm^4]. The calculated result in the present model is $B(E0{:}\mathrm{IS})=92$ fm^4, in good agreement with the experimental data. On the other hand, the AMD calculation also reproduces the experimental data [$B^{\mathrm{AMD}}(E0{:}\mathrm{IS})=94$ fm^4]. They analyzed the density distributions of the ground state and excited states in ^{11}B and ^{12}C and concluded that the $3/2_3^-$ state in ^{11}B is a dilute cluster state, and its features are similar to those of the Hoyle state ^{12}C(0_2^+), which is likely to be a gas state of 3α clusters. However, it is not self-evident in the AMD calculation whether the $3/2_3^-$ state possesses an α-condensate nature like the Hoyle state having about 70% probability of the α particle occupied in a single S orbit. To see the single-cluster properties in ^{11}B, we study the single-cluster orbits and their occupation

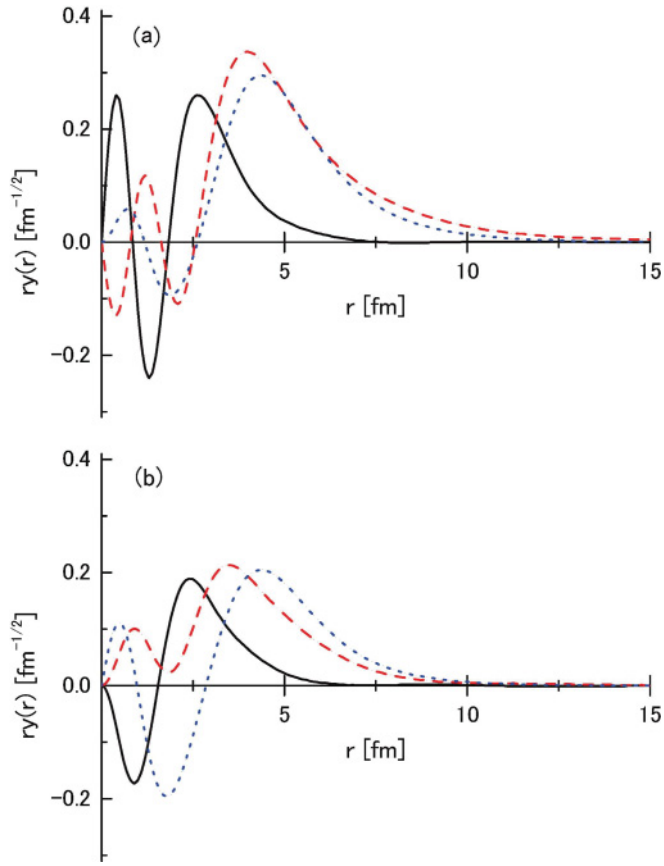

FIG. 3. (Color online) Reduced width amplitudes or overlap amplitudes of the (a) ^{7}Li$(3/2^-;\mathrm{g.s})+\alpha$ and (b) ^{8}Be$(0^+;\mathrm{g.s})+t$ channels in the $3/2_1^-$ (solid line) and $3/2_3^-$ (dashed line) states of ^{11}B. The relative angular momentum of the amplitudes are $\ell_{74}=0$ for (a) and $j_{83}=3/2^-$ for (b). The dotted lines in (a) and (b) represent, respectively, the reduced width amplitudes of ^{7}Li$(3/2^-;\mathrm{g.s})+\alpha$ ($\ell=1$) and ^{8}Be$(0^+{:}\mathrm{g.s})+t$ ($\ell=0$) in the $1/2_1^+$ state.

probabilities in the $3/2_3^-$ state by solving the eigenvalue equation of the single-cluster density matrices in Eqs. (12) and (13) and compare them with those in the Hoyle state.

Figure 4 shows the occupation probabilities of the nth L-wave single-α-particle (single-t-particle) orbits in the $3/2_1^-$ and $3/2_3^-$ states (see also Table II). In the $3/2_1^-$ state, the occupation probabilities of the single-α-particle orbits spread out in several orbits. These features can be understood from the fact that the $3/2_1^-$ state has the dominant configuration of SU(3)$[f](\lambda,\mu)_L=[443](1,3)_1$ ($Q=7$) coupled with the spin of the t-cluster. In fact, the SU(3) wave function is expressed in terms of the harmonic oscillator basis $|(n_{44}\ell_{44})\otimes(n_{83}\ell_{83})\rangle$,

$$
\begin{aligned}
&|[443](1,3)_{L=1}\rangle \\
&\quad=\sqrt{\frac{64}{225}}|(2S)\otimes(1P)\rangle-\sqrt{\frac{56}{225}}|(1D)\otimes(1P)\rangle \\
&\qquad-\sqrt{\frac{24}{225}}|(1D)\otimes(0F)\rangle+\sqrt{\frac{81}{225}}|(0G)\otimes(0F)\rangle, \qquad (23)
\end{aligned}
$$

where $(n_{44}\ell_{44})$ [$(n_{83}\ell_{83})$] represents the harmonic oscillator wave function, n and ℓ denoting the number of nodes and

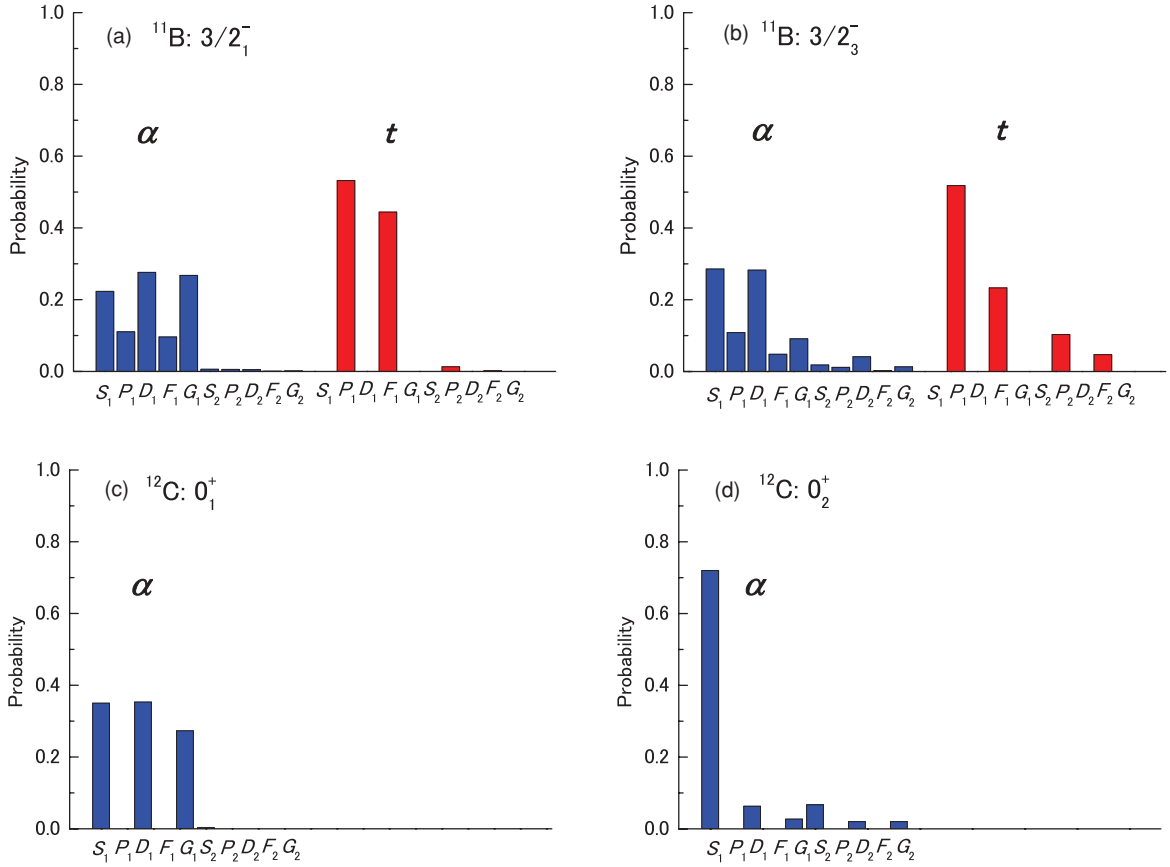

FIG. 4. (Color online) Occupation probabilities of the single-α-particle and single-t-particle orbits for the (a) $3/2^-_1$ (g.s.) and (b) $3/2^-_3$ states in ^{11}B. For reference, we show those of the single-α-particle orbits for the (c) 0^+_1 (g.s.) and (d) 0^+_2 (Hoyle) states in ^{12}C calculated by the 3α OCM [9]. The specific numbers of the occupation probabilities for the L_1 orbits are given in Table II. Note that the occupation probability of the L_n orbit with $n \geqslant 2$ is less than 0.05.

the orbital angular momentum, respectively, with respect to the relative coordinate $\boldsymbol{r}_{44}$ between the two α clusters ($\boldsymbol{r}_{83}$ between the 2α and t clusters). From the definition of the single-α-particle density matrix in Eq. (12), one obtains the occupation probabilities as follows: 22.3%, 11.4%, 28.0%, 10.0%, and 28.3% for S_1, P_1, D_1, F_1, and G_1 orbits, respectively. These results agree well with those in Fig. 4 and Table II. The radial behaviors of the S_1-, D_1-, and G_1-wave single-α-particle orbits as well as the P_1 and F_1 orbits are shown in Fig. 5(a). One sees strong oscillations in the inner regions, coming from the strong Pauli-blocking effect, reflecting the nature of the compact shell-model-like structure

TABLE II. Occupation probabilities of the single-α-particle and single-t-particle orbits for $3/2^-_1$ (g.s.), $3/2^-_3$, $1/2^+_1$, and $1/2^+_2$ in ^{11}B. For reference, we show those of the single-α-particle orbits for 0^+_1 (g.s.) and 0^+_2 (Hoyle) in ^{12}C [9]. In the table, "Others" means orbits higher than those shown in the table. The reasons why the single-t-particle occupation probability with odd (even)-parity orbits is exactly zero in $3/2^-$ ($1/2^+$) are given in the text.

Nucleus	J^π	Orbits	S_1	P_1	D_1	F_1	G_1	Others
	$3/2^-_1$	α	0.223	0.111	0.276	0.096	0.268	0.026
		t	–	0.532	–	0.444	–	0.024
	$3/2^-_3$	α	0.286	0.109	0.283	0.048	0.091	0.183
^{11}B		t	–	0.518	–	0.233	–	0.249
	$1/2^+_1$	α	0.070	0.333	0.051	0.298	0.034	0.214
		t	0.325	–	0.198	–	0.019	0.458
	$1/2^+_2$	α	0.519	0.180	0.035	0.036	0.015	0.215
		t	0.933	–	0.026	–	0.004	0.037
^{12}C	0^+_1	α	0.350	–	0.353	–	0.273	0.024
	0^+_2	α	0.720	–	0.063	–	0.027	0.190

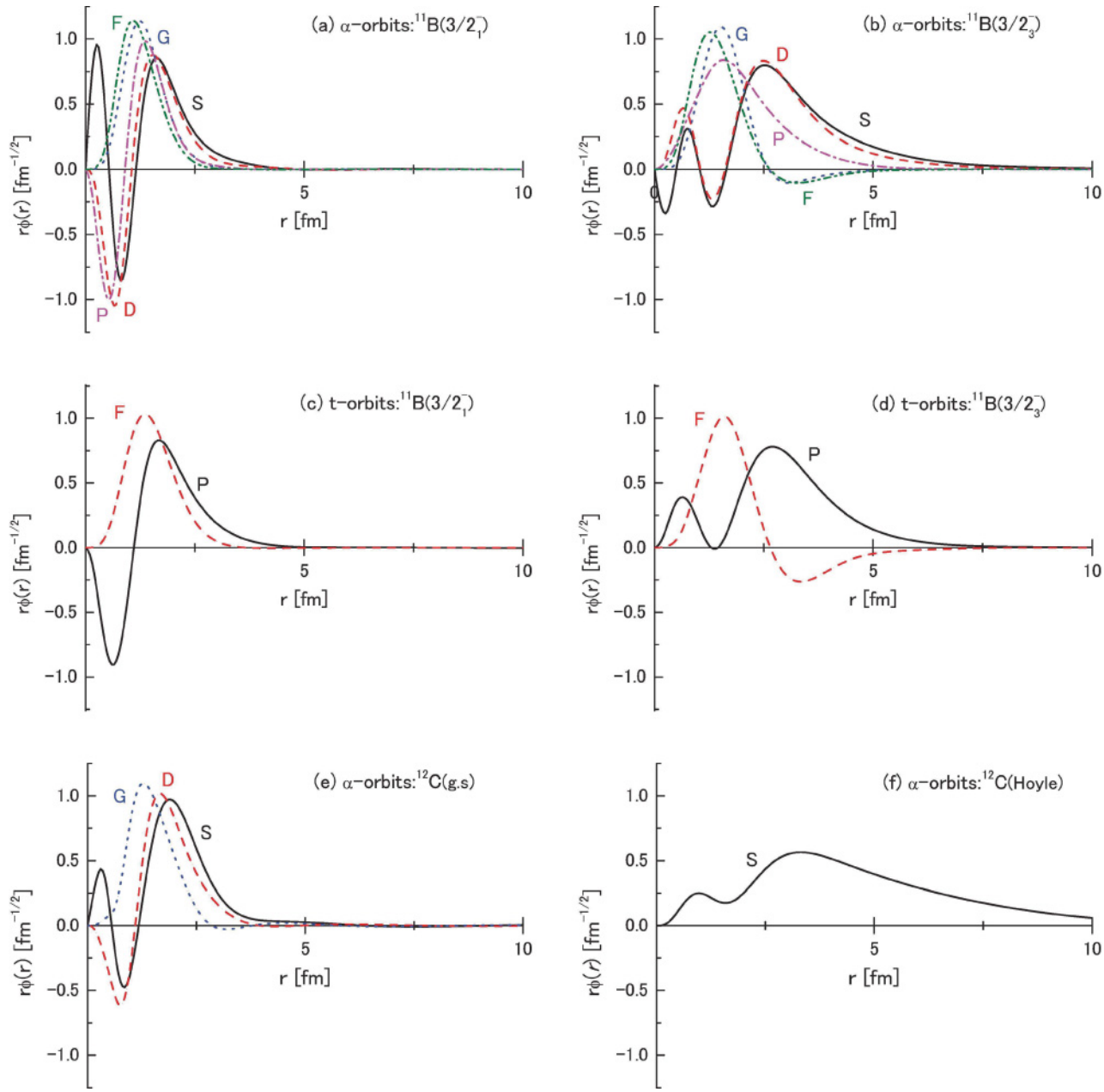

FIG. 5. (Color online) Radial behaviors of the single-α-particle orbits in the (a) $3/2^-_1$ and (b) $3/2^-_3$ states, where the solid line (dashed, dotted, dash-dotted, and dash-two-dotted) denotes the S_1 wave (D_1, G_1, P_1, and F_1, respectively), and those of the single-t-particle orbits in the (c) $3/2^-_1$ and (d) $3/2^-_3$ states, where the solid line (dashed) denotes the P_1-wave (F_1-one) [see Figs. 4(a) and (b)]. For reference, those of the single-α-particle orbits in the (e) ground state of ^{12}C and (f) Hoyle state are shown [9], where the solid line (dashed and dotted) denotes the S_1 wave (D_1 and G_1, respectively). [see Figs. 4(a) and (b)].

in this state. These behaviors are quite similar to those of the ground state of ^{12}C shown in Fig. 5(e) [9], the structure of which is shell-model-like [2–4,13].

On the other hand, the single-t-particle occupation probabilities in the $3/2^-_1$ state concentrate mainly on the two orbits, P_1 and F_1 [see Fig. 4(a) and Table II]. These results originate from the SU(3) nature of the $3/2^-_1$ state. In fact, the definition of the single-t-particle density matrix in Eq. (13) gives 53.3% for the P orbit and 46.7% for the F orbit, when one uses the SU(3) wave function in Eq. (23). The reason why the single-t-particle probability with odd parity is exactly zero in $3/2^-$ is due to the symmetric nature of the total wave function of ^{11}B in Eq. (1). In fact, the symmetric character in Eq. (1) with respect to the exchange between two α clusters causes even-parity orbital angular momentum between the two α's and, thus, only odd-parity-wave single-t-particle orbits are allowed in the negative-parity ^{11}B state. This is discussed in detail in the case of ^{12}C with the 3α OCM (see Ref. [9]). The radial behavior of the P-wave single-t-particle orbit in Fig. 5(c) indicates a strong oscillation in the inner region, reflecting the compact shell-model-like feature of the $3/2^-_1$ state.

As for the $3/2_3^-$ state possessing an $\alpha + \alpha + t$ cluster structure, the occupation probabilities of the single-α-particle orbits have *no* concentration on a single orbit [see Fig. 4(b) and Table II]. One notices that $P^{(\alpha)}(S_1) \sim P^{(\alpha)}(D_1) \sim 30\%$, where $P^{(\alpha)}(L_n)$ denotes the occupation probability for nth L-wave α orbit. It is noted that there is a close relation between the occupation probability $P^{(\alpha)}$ and the S^2 factor of the α reduced width amplitudes, as discussed in Ref. [9]. In fact, in the present calculation, the S-wave and D-wave S^2 factors of the $^7\mathrm{Li} + \alpha$ reduced width amplitudes in $3/2_3^-$ amount to 0.26 and 0.29, respectively, the ratio of which is similar to $P^{(\alpha)}(S_1)/P^{(\alpha)}(D_1) \sim 1$.

The radial behaviors of the single-α-particle S_1, D_1, and G_1 orbits are shown in Fig. 5(b). Compared with the results of the ground state [see Fig. 5(a)], the strong oscillation in the inner region is rather suppressed, although the outermost peak is enhanced in the $3/2_3^-$ state. For reference, we show in Fig. 5(f) the S-wave single-α-particle orbit in the Hoyle state of ^{12}C [9] (which is a typical example of α condensation in nuclei), where the α particle occupies the S orbit with about 70% probability. In this Hoyle state, one sees no nodal behaviors (but small oscillations) in the inner region together with a long tail, and the radial behavior is likely to be of the $0S$-type Gaussian. This Gaussian behavior and its occupation probability as large as about 70% are the evidence that the Hoyle state has a 3α-condensate structure [7,9,10]. Comparing them with the case of the $3/2_3^-$ state in ^{11}B, we find remarkable qualitative differences between them: (1) the $3/2_3^-$ state has no concentration of occupation probability on a single-α-particle orbit and (2) nodal behaviors remain in the inner region in $3/2_3^-$, indicating a rather large Pauli-blocking effect. These results show that the $3/2_3^-$ state does not have α-condensate nature like the Hoyle state.

Concerning the single-t-particle motions in $3/2_3^-$, the P_1 orbit has the largest probability of 51.8%. The radial behavior of the P_1 orbit is shown in Fig. 5(d), and it has no nodal behaviors but somewhat largely oscillating behaviors in the inner region, in contrast with the case of the single-α-particle orbits. The reason why the nodal behavior disappears is due to the fact that the rms distance between the center-of-mass of 2α and the triton is as large as $R_{^8\mathrm{Be}-t} \simeq 3.4$ fm (see Table I), and thus the Pauli-blocking effect is weakened significantly to make the small oscillation in the inner region.

From the abovementioned results, the $3/2_3^-$ state could not be described by the product states of clusters, although its state has the $\alpha + \alpha + t$ cluster structure. The essential reason why the $3/2_3^-$ state does not have the nature of the cluster product states is due to the fact that the $3/2_3^-$ state is bound by 2.9 MeV with respect to the $\alpha + \alpha + t$ threshold, while the Hoyle state appears by 0.38 MeV above the 3α threshold; that is, the energy level is located around the Coulomb barrier produced by the clusters. This extra binding energy of the $3/2_3^-$ state with respect to the three-body threshold hinders significantly the development of the gas-like $\alpha + \alpha + t$ structure with a large nuclear radius in the state. In Refs. [7,19], the authors discussed important requirements for the emergence of the cluster-gas states with a large radius, in which all the clusters occupy an $0S$ orbit, and thus its dominant configuration is $(0S)^n$ (n denotes the number of the clusters): (1) The state should be located above the constituent cluster threshold to make a dilute cluster structure with a large nuclear radius, that is, it should appear around the Coulomb barrier produced by the relevant constituent clusters, and (2) all of the clusters interact dominantly in S-wave with each other to avoid the Pauli-blocking effect among the clusters as well as to reduce the effect of the centrifugal barrier among them. These are *the necessary conditions for the appearance of the cluster product states*. These conditions are not fulfilled in the $3/2_3^-$ state as discussed in the present study. Thus, the $3/2_3^-$ state does not have the cluster-product-state nature.

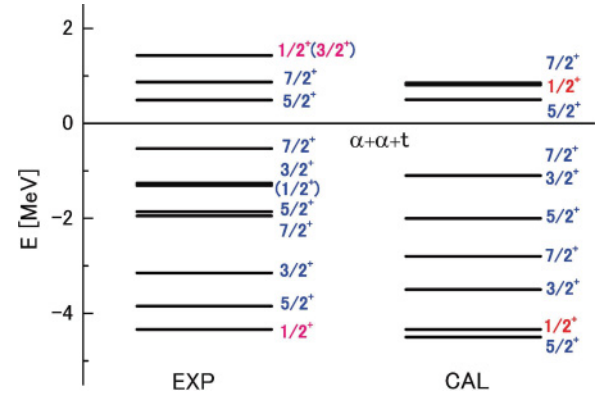

FIG. 6. (Color online) Calculated energy levels of the positive-parity states in ^{11}B with respect to the $\alpha + \alpha + t$ threshold together with the experimental data [36].

B. $1/2^+$ states

The positive-parity levels of ^{11}B obtained by the present $\alpha + \alpha + t$ OCM calculation are shown in Fig. 6 (only $1/2^+$ states as well as $3/2^-$ states are given in Fig. 2). The $1/2_1^+$, $3/2_1^+$, and $5/2_1^+$ states are stable against any particle decays. Other calculated states correspond to resonant states that are identified with use of the CSM, as explained in Sec. II B. One can see rather good correspondence to the experimental data. In the present article, we concentrate on studying the structure of $1/2^+$ states. The structures of other positive-parity states will be discussed elsewhere, although we found that some even-parity states shown in Fig. 6 have cluster structures.

The calculated nuclear radius of $1/2_1^+$ is $R_N = 2.82$ fm. This value is similar to the $3/2_3^-$ state, which has the $\alpha + \alpha + t$ cluster structure (see Table I). Figure 3(a) shows the reduced width amplitude or overlap amplitude for the $^7\mathrm{Li}(3/2^-; \mathrm{g.s}) + \alpha$ channel with the relative orbital angular momentum $\ell_{74} = 1$. One sees that the shape of the outermost peak at $r \sim 5$ fm is similar to that of $3/2_3^-$. The S^2 factor for this channel is 0.203. This is the largest among all of the $^7\mathrm{Li} + \alpha$ channels with $^7\mathrm{Li}(\mathrm{g.s}, 1/2^-, 7/2^-, 5/2^-)$, where the corresponding S^2 factors are 0.203, 0.099, 0.120, and 0.047, respectively. As for the $^8\mathrm{Be} + t$ channel, the S^2 factor for $^8\mathrm{Be}\,(\mathrm{g.s}) + t$ [$^8\mathrm{Be}(2^+) + t$] is 0.130 (0.134). The reduced width amplitude of the $^8\mathrm{Be}(\mathrm{g.s}) + t$ channel is shown in Fig. 3(b). On the other hand the α–t distance ($^7\mathrm{Li} - \alpha$) in $1/2_1^+$ is $R_{\alpha-t} = 3.81$ fm ($R_{^7\mathrm{Li}-\alpha} = 3.45$ fm). This value is a little bit larger than that of the ^{7}Li ground state ($R_{\alpha-t} = 3.5$ fm)

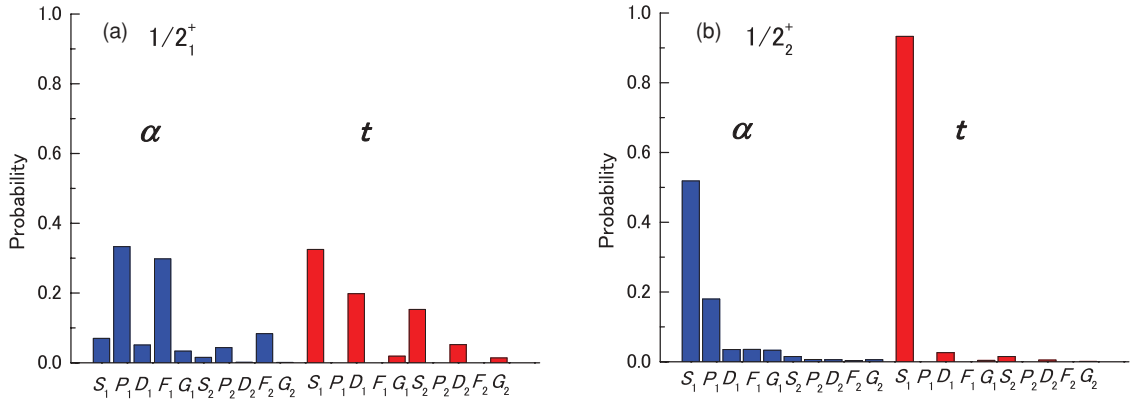

FIG. 7. (Color online) Occupation probabilities of the single-α-particle and single-t-particle orbits for the (a) $1/2^+_1$ and (b) $1/2^+_2$ states in ^{11}B.

obtained by the $\alpha + t$ OCM calculation. Thus, the $1/2^+_1$ state has a dominant structure of ^{7}Li(g.s) + α with P-wave relative motion. As discussed in Sec. III A, the $3/2^-_3$ state has the largest S^2 factor for the ^{7}Li(g.s) + α channel with S-wave relative motion. This means that the state includes significantly the structure of ^{7}Li(g.s) + α. In the nonidentical two-cluster states, for example, in the ^{16}O + α states of ^{20}Ne, there appear the parity-doublet states, 0^+ and 1^-, around the ^{16}O + α threshold, in which the relative motion between ^{16}O and α is of the S wave and P wave, respectively [2,45]. Thus, the $1/2^+_1$ and $3/2^-_3$ states of ^{11}B, which are located around the ^{7}Li(g.s) + α threshold, can be interpreted as the parity doublet in ^{11}B.

The occupation probabilities of the single-α-particle and single-t-particle orbits for $1/2^+_1$ are shown in Fig. 7(a) (see also Table II). The P_1 (F_1) orbit of the α particle has the largest (secondarily largest) occupation probability of 33% (30%). One sees a close relationship between the cluster occupation probabilities and the S^2 factors (as well as one between the single-cluster orbits and the reduced width amplitudes): (1) the S^2 factor of ^{7}Li(g.s) + α with $\ell_{74} = 1$ ($\ell_{74} = 3$) is the largest (second largest) among all of the ^{7}Li + α channels, as discussed above, and (2) the radial behavior of the P_1 orbit in Fig. 9(a) is similar to that of the reduced width amplitude of the ^{7}Li(g.s) + α channel in Fig. 3(a). It should be noted that the occupation probabilities satisfy with a sum rule, while the S^2 factors do not. On the other hand, the occupation probabilities of single-t-particle orbits spread out over three orbits, S, D, and G. This feature is similar to the results of the S^2 factors for the ^{8}Be + t channels. The reason why the odd-parity t-orbit occupation probabilities are exactly zero comes from a symmetric feature of the $\alpha + \alpha + t$ cluster model with respect to the exchange of the two α's, as mentioned before. The present results indicate that the $1/2^+_1$ state does not correspond to the product states of clusters, in which all clusters dominantly occupy the $0S_\alpha$ orbit. The main reason why the $1/2^+_1$ state does not have a dilute structure like the Hoyle state is due to the fact that $1/2^+_1$ is bound by 4.2 MeV with respect to the $\alpha + \alpha + t$ threshold. This fact hinders strongly the growth of a gas-like $\alpha + \alpha + t$ structure in $1/2^+_1$.

The CSM with the $\alpha + \alpha + t$ OCM is a powerful tool to identify resonant states, in particular, those around the $\alpha + \alpha + t$ threshold. Figure 8 displays the energy eigenvalues obtained by solving the complex-scaled Schrödinger equation in Eq. (20) with $2\theta = 18^\circ$ (θ denotes the scaling angle). As explained in Sec. II B, one can identify bound states and resonances as stationary points independently of θ. In the present study, in addition to the bound $1/2^+_1$ state, we found that the $1/2^+_2$ state appears at $E_x = 11.85$ MeV, ($E = 0.75$ MeV just above the $\alpha + \alpha + t$ threshold), as a resonant state with the width of $\Gamma = 190$ keV. It is reminded that the Hoyle state [^{12}C(0^+_2)] appears at 0.38 MeV above the 3α threshold and has the very small width of $\Gamma = 8.5 \pm 1.0$ eV.

It is instructive to study the structure of the $1/2^+_2$ state under the bound-state approximation, because the calculated width is small. We found that the calculated nuclear radius of $1/2^+_2$ is 5.93 fm, the value of which is significantly larger than that of $1/2^+_1$. This means that the $1/2^+_2$ state has a dilute cluster structure. To study the structure further, we calculated the occupation probabilities and radial behaviors of the

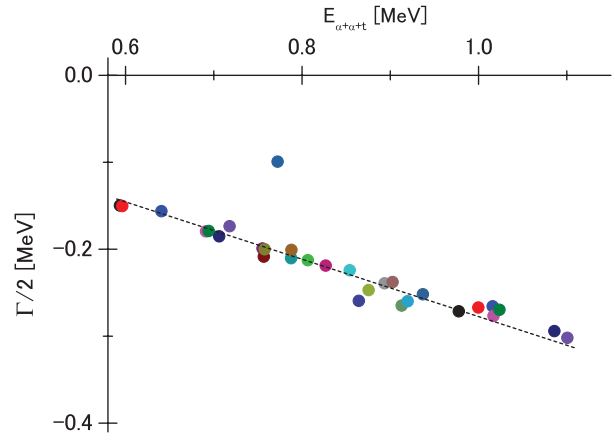

FIG. 8. (Color online) Energy eigenvalues of $1/2^+$ states obtained by solving the complex-scaled Schrödinger equation in Eq. (20) with $2\theta = 18^\circ$. The real energy $E_{\alpha+\alpha+t}$ is measured from the $\alpha + \alpha + t$ threshold. In this figure, only the energy region of 0.6 MeV $\leqslant E_{\alpha+\alpha+t} \leqslant$ 1.2 MeV is shown. A stationary point at $E = (0.75, -0.095)$, independent of the value of θ, gives the resonance parameters. Other points correspond to the discretized $\alpha + \alpha + t$ and ^{8}Be(0^+) + t continuum states with $2\theta = 18^\circ$, which are located around the dotted line of $2\theta = 18^\circ$.

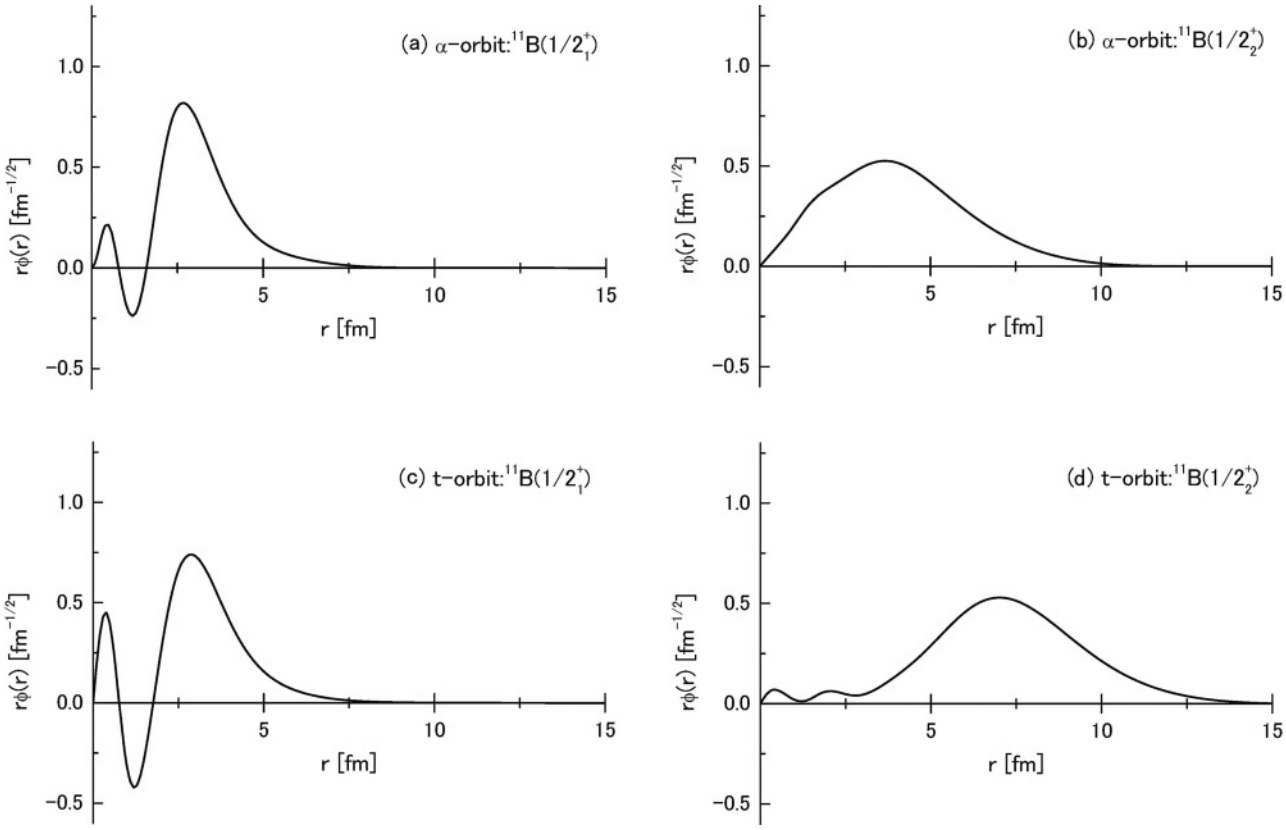

FIG. 9. Radial behaviors of the single-α-particle orbits in the $1/2^+_1$ and $1/2^+_2$ states: (a) P_1 wave of $1/2^+_1$ with the largest occupation probability $P^{(\alpha)}(P_1) = 33\%$ and (b) S_1 wave of $1/2^+_2$ with $P^{(\alpha)}(S_1) = 52\%$ [see Figs. 7(a) and (b)]. Those of the single-t-particle orbits in the two $1/2$ states are shown in (c) for the S_1 wave of $1/2^+_1$ with the largest occupation probability $P^{(t)}(S_1) = 33\%$ and in (d) for the S_1 wave of $1/2^+_2$ with $P^{(t)}(S_1) = 93\%$.

single-α-particle and single-t-particle orbits by diagonalizing the single-cluster density matrices defined in Eqs. (10) and (11). The results are shown in Fig. 7(b). We see that the occupation probability of the S_1-wave α orbit (S_α) is as large as about 52%, and that of the S_1-wave t orbit (S_t) amounts to about 93%. Then the probability of the $(S_\alpha)^2(S_t)$ configuration in $1/2^+_2$ can be estimated to be $1.97/3 \sim 65\%$, where the dominator denotes the total cluster number (3 clusters) and the numerator is the cluster number occupied in the $(0S_\alpha)^2(0S_t)$ configuration, that is, $2 \times 0.55 + 0.93 = 1.97$. The radial behaviors of the S_α orbit and the S_t orbit are depicted in Figs. 9(c) and 9(d), respectively, showing a Gaussian behavior with no nodes. Thus, we could call this state the Hoyle analog, where all clusters are mainly in their respective $0S$ orbits, that is, $(0S_\alpha)^2(0S_t)$ with a probability of about 65%, which is similar to the Hoyle state with the main configuration of $(0S_\alpha)^3$ possessing a probability of about 70%. Note that the present $1/2^+_2$ state satisfies the necessary conditions of the appearance of the product states of clusters as discussed in Sec. III A. The peak position in the S_α orbit (S_t orbit) is around 3.5 fm (7.0 fm). This result means that the triton cluster moves outside of the α clusters. Thus, the $1/2^+_2$ state has a t-halo-like structure around the two α clusters. It should be noted that the S-wave α-α interaction is attractive enough to produce the resonant state of ^{8}Be(g.s), but the S-wave α-t interaction is weakly attractive and has no ability to produce bound/resonant states in ^{7}Li. This qualitative difference makes the t-halo-like structure around the two α clusters in the $1/2^+_2$ state.

Here, it is interesting to discuss the reason why the calculated width of the $1/2^+_2$ state is small ($\Gamma^{\rm cal} = 190$ keV), despite the large excitation energy ($E_x = 11.85$ MeV). The decay width is composed of the contributions from the two-body decays ($^7\mathrm{Li} + \alpha$ and $^8\mathrm{Be} + t$) and the three-body decay ($\alpha + \alpha + t$). As for the three-body decay, it is suppressed strongly due to the very small phase space arising from the fact that the $1/2^+_2$ state is located at 0.75 MeV above the $\alpha + \alpha + t$ threshold. On the other hand, the ^{8}Be(g.s) $+ t$ decay is possible, because its state appears at about 0.7 MeV above the ^{8}Be(g.s) $+ t$ threshold. But, its energy level is located inside the Coulomb barrier (no centrifugal barrier for the S-wave decay of ^{8}Be(g.s) $+ t$), and thus its decay is hindered. As for the $^7\mathrm{Li} + \alpha$ decay, the energy of $1/2^+_2$ measured from the ^{7}Li(g.s:$3/2^-$) $+ \alpha$ threshold is about 3.8 MeV. In this case, the orbital angular momentum of the decaying α particle should be P wave, but the P-wave occupation probability of the α particle in the state is as small as 20% (see Fig. 7). Thus, the P-wave decay of ^{7}Li(g.s) $+ \alpha$ is suppressed largely due to the small occupation probability and the Coulomb and centrifugal barriers. On the contrary, the S-wave decay of $^7\mathrm{Li} + \alpha$ is also possible, because the S-wave occupation probability of

the α particle is about 53%. However, the bound and/or resonant states of positive-parity ^{7}Li states have not been identified experimentally so far in the low-energy region up to $E_x \sim 15$ MeV [40]. This experimental fact indicates a large hindrance of the S-wave $^7\mathrm{Li}+\alpha$ decay with even-parity ^{7}Li states. Consequently the calculated width of the $1/2^+_2$ state becomes small.

It is interesting to discuss the experimental situation on the $1/2^+$ states (isospin $T=1/2$) of ^{11}B around the $\alpha+\alpha+t$ threshold. As mentioned in Sec. I, the $1/2^+(3/2^+)$ state at $E_x = 12.56$ MeV with $\Gamma = 210 \pm 20$ keV (located at 1.4 MeV above the $\alpha+\alpha+t$ threshold), which was identified so far as the isospin $T=3/2$ state [36], has recently been observed through the $\alpha+{}^7$Li decay channel [33–35]. Thus, the latter experiments indicate that the $E_x = 12.56$ MeV state is $T=1/2$. Comparing the experimental results with our present theoretical results, the energy and width of the $1/2^+_2$ state obtained by the present study are in good correspondence with the experimental data. Thus, the present calculated results indicate that the 12.56-MeV state could be assigned as the $1/2^+_2$ state ($T=1/2$), the wave function of which has the nature of *the product states of the clusters,* 2α *and* t, *all in the lowest* $0S$ *orbit*. Our results also support the experimental indication of the 12.56-MeV state being $T=1/2$ [34].

IV. SUMMARY

We have studied the structure of $3/2^-$ and $1/2^+$ states in ^{11}B with the $\alpha+\alpha+t$ OCM using the GEM. The model space covers the description of $^7\mathrm{Li}+\alpha$ and $^8\mathrm{Be}+t$ cluster structures and $\alpha+\alpha+t$ gas-like structures including the shell-model-like structures. Full levels up to $3/2^-_3$ and $1/2^+_2$ around the $\alpha+\alpha+t$ threshold are reproduced. The $3/2^-_1$ (g.s) and $3/2^-_2$ states are found to have the shell-model-like compact structures, the results of which are consistent with the previous cluster model analyses by Nishioka *et al.* [20–22]. The $3/2^-_3$ state is characterized by the monopole transition strength as large as 0^+_2 at $E_x = 7.65$ MeV in ^{12}C. The present study succeeded in reproducing its excitation energy and monopole transition strength. We found that this state has an $\alpha+\alpha+t$ cluster structure with a nuclear radius of $R_N = 3.00$ fm. The study of the single-cluster properties such as single-cluster orbits and occupation probabilities for $3/2^-_3$ showed that there is no concentration of the single-α occupation probability on a single orbit and the radial part of the single-α orbits has nodal behaviors in the inner region, illustrating rather strong Pauli-blocking effect. These results are in contrast with those of the Hoyle state with the dilute 3α-condensate-like character $(0S_\alpha)^3$, in which the α particle occupies a single $0S$ orbit (zero node) with about 70% probability. Consequently the $3/2^-_3$ state could not be identified as a product state of clusters, possessing a dominant gas-like configuration of $(0S_\alpha)^2(0S_t)$. The reason why the $3/2^-_3$ state does not have such a gas-like configuration can be understood from the following facts: The $3/2^-_3$ state is bound by 2.9 MeV with respect to the $\alpha+\alpha+t$ threshold, while the Hoyle state is located by 0.38 MeV above the 3α threshold and has a dilute 3α structure. The extra binding energy of the $3/2^-_3$ state with respect to the $\alpha+\alpha+t$ threshold is likely to suppress strongly the growth of the gas-like $\alpha+\alpha+t$ structure in this state.

As for the $1/2^+$ states, the $1/2^+_1$ state appears as a bound state at $E_x^{\mathrm{exp}} = 6.79$ MeV around the $^7\mathrm{Li}+\alpha$ threshold. This low excitation energy indicates that α-type correlation should play an important role in the state. In fact, we found that the $1/2^+_1$ state with $R_N = 3.14$ fm has the $^7\mathrm{Li(g.s)}+\alpha$ structure with P-wave relative motion, although the $^7\mathrm{Li}(\alpha+t)$ part is rather distorted in comparison with the ground state of ^{7}Li. Because the $3/2^-_3$ state has the largest S^2 factor for the $^7\mathrm{Li(g.s)}+\alpha$ channel with S-wave relative motion compared with those of other $^7\mathrm{Li}+\alpha$ and $^8\mathrm{Be}+t$ channels, the $1/2^+_1$ and $3/2^-_3$ states of ^{11}B can be interpreted as the parity-doublet partners of each other. They are similar to the typical example of the parity doublet, 0^+_1 and 1^-_1 states in ^{20}Ne, with the $^{16}\mathrm{O}+\alpha$ cluster structure [2,45].

In addition to $1/2^+_1$, we found that the $1/2^+_2$ state appears as a resonant state at $E_x = 11.95$ MeV ($\Gamma = 190$ keV) around the $\alpha+\alpha+t$ threshold with CSM. The large radius ($R_N = 5.98$ fm) indicates that the state has a dilute cluster structure. The analysis of the single-cluster properties showed that this state has a main configuration of $(0S_\alpha)^2(0S_t)$ with about 65% probability. Thus, we could call the $1/2^+_2$ state the product states of clusters with $(0S_\alpha)^2(0S_t)$, which is similar to the Hoyle state possessing the main configuration $(0S_\alpha)^3$ with about 70% probability. It should be noted that $1/2^+_2$ is located by 0.75 MeV above the $\alpha+\alpha+t$ threshold, while $1/2^+_1$ is bound by 4.2 MeV with respect to the three-cluster threshold. The latter binding energy leads to the suppression of the development of the gas-like $\alpha+\alpha+t$ structure in $1/2^+_1$, whereas the gas-like structure with a large nuclear radius grows up in $1/2^+_2$ because the state appears above the three-body threshold.

Recently, the $1/2^+(3/2^+)$ state at $E_x = 12.56$ MeV with $\Gamma = 210 \pm 20$ keV (located at 1.4 MeV above the $\alpha+\alpha+t$ threshold) was observed through the $\alpha+{}^7$Li decay channel [33–35]. The experimental energy and width of the 12.56-MeV state ($T=1/2$) are in good correspondence with the present calculated results of the $1/2^+_2$ state. The product states of clusters in ^{11}B, thus, could be assigned as the 12.56-MeV state. In addition, the present study supports the experimental result [34] that the 12.56-MeV state is $T=1/2$, not $T=3/2$ [36].

It is interesting to study the $\alpha+\alpha+{}^3$He cluster structures and product states of the clusters in the ^{11}C mirror nucleus. Their states should correspond to the $3/2^+_3$, $1/2^+_1$, and $1/2^+_2$ states in ^{11}B. The theoretical study is now in progress. The results will be given elsewhere. Since the experimental situation in ^{11}C is not very clear in comparison with the case of ^{11}B, it is highly hoped that the measurements of the monopole transition rates and the decay properties in ^{11}C will be performed in the near future.

ACKNOWLEDGMENTS

The present authors thank H. Horiuchi, K. Ikeda, G. Röpke, P. Schuck, and A. Tohaski for valuable discussions and encouragement. This work was partially supported by JSPS (Japan Society for the Promotion of Science) Grant-in-Aid for Scientific Research (C) (21540283) and Young Scientists (B) (21740209).

[1] K. Wildermuth and Y. C. Tang, *A Unified Theory of the Nucleus* (Vieweg, Braunschweig, 1977).

[2] K. Ikeda, H. Horiuchi, and S. Saito, Prog. Theor. Phys. Suppl. **68**, 1 (1980).

[3] E. Uegaki, S. Okabe, Y. Abe, and H. Tanaka, Prog. Theor. Phys. **57**, 1262 (1977); E. Uegaki, Y. Abe, S. Okabe, and H. Tanaka, *ibid.* **59**, 1031 (1978); **62**, 1621 (1979).

[4] Y. Fukushima and M. Kamimura, in *Proceedings of the International Conference on Nuclear Structure*, Tokyo, 1977, edited by T. Marumori [J. Phys. Soc. Jpn. Suppl. **44**, 225 (1978)]; M. Kamimura, Nucl. Phys. A **351**, 456 (1981).

[5] T. Yamada, Y. Funaki, H. Horiuchi, K. Ikeda, and A. Tohsaki, Prog. Theor. Phys. **120**, 1139 (2008).

[6] A. Tohsaki, H. Horiuchi, P. Schuck, and G. Röpke, Phys. Rev. Lett. **87**, 192501 (2001).

[7] Y. Funaki, H. Horiuchi, W. von Oertzen, G. Röpke, P. Schuck, A. Tohsaki, and T. Yamada, Phys. Rev. C **80**, 064326 (2009).

[8] Y. Funaki, A. Tohsaki, H. Horiuchi, P. Schuck, and G. Röpke, Phys. Rev. C **67**, 051306(R) (2003).

[9] T. Yamada and P. Schuck, Eur. Phys. J. A **26**, 185 (2005).

[10] H. Matsumura and Y. Suzuki, Nucl. Phys. A **739**, 238 (2004).

[11] P. Schuck, Y. Funaki, H. Horiuchi, G. Röpke, A. Thosaki, and T. Yamada, Prog. Part. Nucl. Phys. **59**, 285 (2007).

[12] Y. Funaki, H. Horiuchi, G. Röpke, P. Schuck, A. Tohsaki, and T. Yamada, Phys. Rev. C **77**, 064312 (2008).

[13] M. Chernykh, H. Feldmeier, T. Neff, P. von Neumann-Cosel, and A. Richter, Phys. Rev. Lett. **98**, 032501 (2007).

[14] Y. Funaki, T. Yamada, H. Horiuchi, G. Röpke, P. Schuck, and A. Tohsaki, Phys. Rev. Lett. **101**, 082502 (2008).

[15] S. Saito, Prog. Theor. Phys. **40**, 893 (1968); **41**, 705 (1969); Prog. Theor. Phys. Suppl. **62**, 11 (1977).

[16] F. Hoyle, Astrophys. J. Suppl. **1**, 121 (1954).

[17] C. W. Cook, W. A. Fowler, C. C. Lauritsen, and T. B. Lauritsen, Phys. Rev. **107**, 508 (1957).

[18] A. Tohsaki, H. Horiuchi, P. Schuck, and G. Röpke, Nucl. Phys. A **738**, 259 (2004).

[19] T. Yamada and P. Schuck, Phys. Rev. C **69**, 024309 (2004).

[20] H. Nishioka, S. Saito, and M. Yasuno, Prog. Theor. Phys. **62**, 424 (1979).

[21] H. Furutani, H. Kanada, T. Kaneko, S. Nagata, H. Nishioka, S. Okabe, S. Saito, T. Sakuda, and M. Seya, Prog. Theor. Phys. Suppl. **68**, 193 (1980).

[22] In Refs. [20,21], the calculated energy levels of the $3/2_3^-$ and $1/2_2^+$ states are not shown in their figures, because the numerical convergence was not enough to obtain definite results. But, they discuss the results with switching off the spin-orbit potentials between the α and t clusters. In this case, they could have rather numerically stable results for the $L^\pi = 1_2^-$ and 0_2^+ states corresponding, respectively, to the $J^\pi = 3/2_3^-$ and $1/2_2^+$ states with $\boldsymbol{J} = \boldsymbol{L} + \frac{1}{2}$, with $\frac{1}{2}$ denoting the spin of the t cluster, as shown in Fig. 2 in Ref. [20]. Then, they discuss the structures of $L^\pi = 1_2^-$ and 0_2^+ in Sec. 3.3 of Ref. [20].

[23] T. Kawabata *et al.*, Phys. Lett. B **646**, 6 (2007).

[24] Y. Kanada-En'yo, Phys. Rev. C **75**, 024302 (2007).

[25] Y. Suzuki and M. Takahashi, Phys. Rev. C **65**, 064318 (2002).

[26] T. Yamada, Y. Funaki, H. Horiuchi, G. Röpke, P. Schuck, and A. Tohsaki, Phys. Rev. A **78**, 035603 (2008); Phys. Rev. C **79**, 054314 (2009).

[27] T. Yamada and Y. Funaki, Int. J. Mod. Phys. E **17**, 2101 (2008).

[28] E. Hiyama, M. Kamimura, T. Motoba, T. Yamada, and Y. Yamamoto, Prog. Theor. Phys. **97**, 881 (1997).

[29] E. Hiyama and T. Yamada, Prog. Part. Nucl. Phys. **63**, 339 (2009).

[30] M. Kamimura, Phys. Rev. A **38**, 621 (1988).

[31] E. Hiyama, Y. Kino, and M. Kamimura, Prog. Part. Nucl. Phys. **51**, 223 (2003).

[32] P. Navrátil, S. Quaglioni, I. Stetcu, and B. R. Barrett, J. Phys. G **36**, 083101 (2009).

[33] N. Soić *et al.*, Nucl. Phys. A **742**, 271 (2004).

[34] N. Curtis, N. I. Ashwood, W. N. Catford, N. M. Clarke, M. Freer, D. Mahboub, C. J. Metelko, S. D. Pain, N. Soić, and D. C. Weisser, Phys. Rev. C **72**, 044320 (2005).

[35] R. J. Charity *et al.*, Phys. Rev. C **78**, 054307 (2008).

[36] F. Ajzenberg-Selove, Nucl. Phys. A **506**, 1 (1990).

[37] In the present calculation, we take the Gaussian parameters in Eq. (4) as follows: $b = 0.60$ (0.30) fm and $b_{n_{\max}} = 7.00$ (8.00) fm with $n_{\max} = 10$ for $3/2^-$ ($1/2^+$) states.

[38] V. I. Kukulin, V. M. Krasnopol'sky, V. T. Voronchev, and P. B. Sazonov, Nucl. Phys. A **417**, 128 (1984).

[39] A. Hasegawa and S. Nagata, Prog. Theor. Phys. **45**, 1786 (1971); F. Tanabe, A. Tohsaki, and R. Tamagaki, *ibid.* **53**, 677 (1975).

[40] F. Ajzenberg-Selove, Nucl. Phys. A **490** 1, (1988).

[41] J. Aguilar and J. M. Combes, Commun. Math. Phys. **22**, 269 (1971); E. Balslev and J. M. Combes, *ibid.* **22**, 280 (1971); B. Simon, *ibid.* **27**, 1 (1972).

[42] A. T. Kruppa, R. G. Lovas, and B. Gyarmati, Phys. Rev. C **37**, 383 (1988).

[43] A. T. Kruppa and K. Katō, Prog. Theor. Phys. **84**, 1145 (1990).

[44] S. Aoyama, T. Myo, K. Katō, and K. Ikeda, Prog. Theor. Phys. **116**, 1 (2006).

[45] H. Horiuchi and K. Ikeda, Prog. Theor. Phys. **40**, 277 (1968).